Reconfigurable Large-Scale Pattern Formation Driven by Topological Defect Separation in Liquid Crystals

Satoshi Aya,* Peter Salamon, Nandor Eber, Agnes Buka, and Fumito Araoka*

Large-scale patterning of topological defects is vital and challenging from both fundamental and technological points of view in anisotropic fluids. However, this is usually difficult because of their unfavorably high-energy states. Here, a simple but general pathway for topology engineering is presented: processing topological defects and shape large-scale patterns in materials with liquid crystalline nature. Dragging field is created through flowing materials at liquid–liquid crystal phase transition temperature or designing electric-field driven temperature gradient. The dragging fields coupled to a dense colony of topological defects with random spatial distribution form nontrivial periodic ordered topological patterns that are energetically unfavorable compared to the uniform ground state, but are stable in the stationary state. Topological polymeric films based on the strategy are also fabricated. The dragging speed and surface interactions are found to be dominant factors in generating and stabilizing the patterns. This strategy endows fluids with regular and large-scale topological patterns, paving a new way for the development of fluids and gels with spatially modulated topological nature.

Topological defects[1] (TDs) represent homotopic or geometric singularities in materials, and they appear when continuity in shape, structure, and orientation of material constituents are lost. From fundamental point of view, TDs have been proven to play key roles in many phenomena in condensed matter physics, e.g., phase transitions,[2] quantum effects,[3] structural formation[4] and the like. In recent decades, the importance of TDs for realizing new technologies in the field of optics, mechanics and spintronics has increased significantly,[5–10]

although they are considered as unfavorable elements since the existence of TDs lowers performance of many modern technologies, such as solar cells and liquid crystal displays. While TDs are less mobile in solid-state materials, they can flow in fluids, thus providing opportunities for manipulating TDs. Indeed, it is found that the fundamental interactions existing between TDs in anisotropic fluids such as liquid crystals can be controlled and result in a diversity of exotic structures in colloid science.[11–13] Therefore, mobile TDs offer a multifaceted playground for understanding fundamental topology-dependent dynamics and testing potential topological manipulation.

Particular focuses and challenges of this work are to present a new dynamic pattern forming process of TDs at a large-scale, up to millimeter, when a swarm of TDs are coupled to an external dragging field, and to memorize the patterns in the systems at the equilibrium. The recent development in the control of TDs has been devoted to manipulating and organizing nano/microscopic objects through adjusting interactions between TDs and the objects.[11–15] In these cases, TDs are prepared in an indirect way, where micro-objects such as colloidal particles are employed as seeds of topological defects, generating diverse static configurations of colloidal self-assemblies in dependence on the type of topological variants of each colloidal particle. Another mainstream is designing permanent topological patterns through pre-photopatterning interfacial orientation[16,17] or microfluidic manipulation[18] in a top-down manner. Usually, systems without the alien micro-objects, flow and the interfacial patterning prefer a defect-free state because the existence of TDs costs elastic free energy, thus promoting the annihilation of TDs in the stationary state when released from an external field.[19–29] Such examples can be found in pattern formation of liquid crystals caused by electroconvective instabilities, where the topological patterns generated by short-distance circulative flow at nonequilibrium state relax back to the uniform ground state,[30] and also by flow under an oscillatory flow field or flexoelectric effect under an electric field.[31,32] In this regard, topological pattern formation retained at the final stationary state in a self-assembling manner is thought-invoking and remains unraveled. In this article, we propose a strategy to develop large-scale production of topological patterns in fluids up to centimeter scale without any template material or prior surface treatments. By artificially creating dragging force

Prof. S. Aya
South China Advanced Institute for Soft Matter Science and Technology (AISMST)
South China University of Technology
Guangzhou 510640, China
E-mail: satoshiaya@scut.edu.cn

Dr. P. Salamon, Dr. N. Eber, Prof. A. Buka
Institute for Solid State Physics and Optics
Wigner Research Center for Physics
P. O. Box 49, Budapest H-1525, Hungary

Dr. F. Araoka
Physicochemical Soft Matter Research Team
RIKEN Center for Emergent Matter Science (CEMS)
Saitama 351-0198, Japan
E-mail: fumito.araoka@riken.jp

The ORCID identification number(s) for the author(s) of this article can be found under https://doi.org/10.1002/admi.202000139.
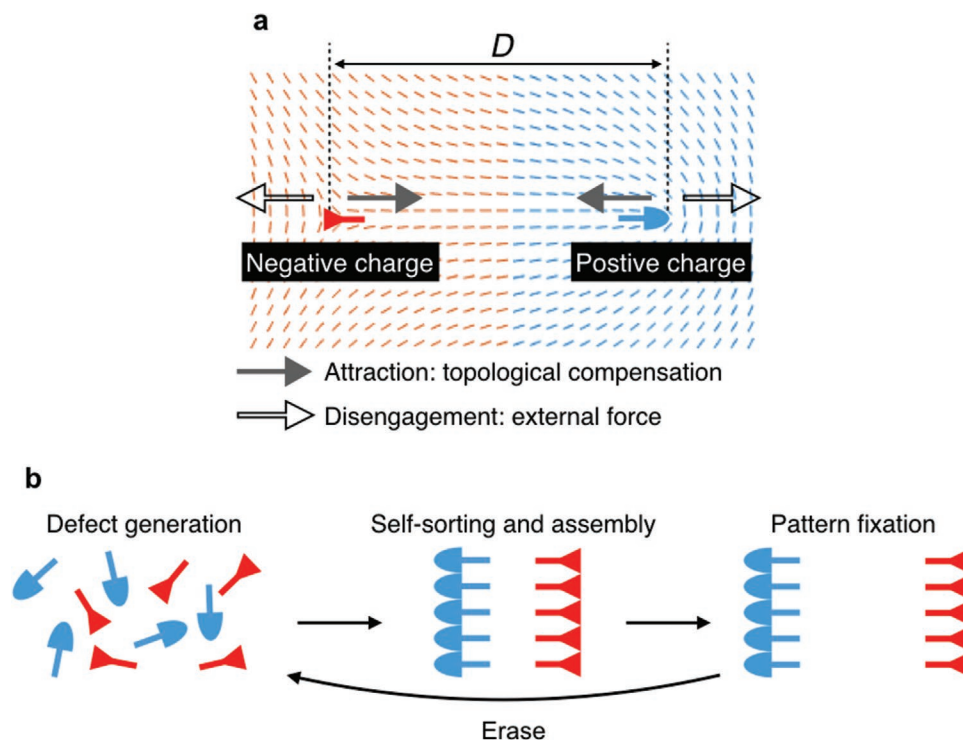
Figure 1. Concept of processing a swarm of topological defects to a large-scale. a) Forces acting on a pair of topological defects with opposite topological charges (blue: $s = +1/2$, red: $s = -1/2$). b) Schematics of the strategy of generating topological pattern from a swarm of topological defects.

in space, which prevents the annihilation process and enables self-sorting and alignment of TDs, we succeeded in realizing nontrivial topological patterns that are stabilized by the balance between interactions of TDs and surface anchoring force of interfacial molecules. These results may generate interests in further understanding of self-assembling dynamics of TDs as well as producing potential applications in regenerable optical elements.

Our strategy is presented in **Figure 1**a,b. The convectional situation is that, when a pair of TDs with opposite signs, e.g., of topological charge $|s| = 1/2$ (corresponding to line defects aligning perpendicular to the substrates), is created from a uniaxial planarly oriented background fluid and separated by a distance of D, they attract each other (solid arrows in Figure 1a) driven by an elastic force, $f_{inter} = 2s_1s_2\pi K/D$ with K being the effective elastic constant and s_i the topological strength. This leads to the vanishing of the topological charges in order to eliminate the energy cost caused by a spatial variation of director orientation about the TDs. When a counter force (open arrows in Figure 1a, e.g., a dragging force) working in the direction opposite to TD–TD direction comes into play, the coalescence of the defects can be avoided under specific conditions, due to the force acting to separate them. Indeed, in many active matter systems, TDs formed by the constituent elements are kept by flow dragging generated by themselves and they form nonvanishing patterns at nonequilibrium.[33] To build an artificial system that mimics the circumstance, we generate a swarm of TDs in liquid crystalline materials (LCs, Experimental Section) by utilizing isotropic liquid–liquid crystal phase transition phenomena. For the subsequent disengagement and assembly

of the TDs, we design and create a dragging field to the LCs by either flowing materials at the liquid-LC phase transition temperature or generating an electric-field driven temperature gradient in the materials upon cooling. The fluidity and flexibility of the LC systems offer erasability and rewritability of the TDs mediated pattern formation as discussed later.

First, we discuss pattern formation by using a flow dragging confined in liquid crystal slabs with degenerate planar surface anchoring. We decrease temperature from the isotropic liquid phase to a nematic (N) LC phase at different cooling rates (2–15 K min⁻¹) upon the application of a dragging field applied by filling the LC material to liquid crystal slabs under the capillary force. In this case, a Poiseuille flow is produced in the liquid crystal slabs. We found that the faster the cooling, the higher the density of randomly oriented TDs generated. **Figure 2**a shows an initial state with a high density of TDs compared to a low-density counterpart. The former generates a large-scale topological pattern by a periodic director arrangement, observed by polarized light microscopy (POM). The dragging is known to flow-align the director of rod-like NLCs.[34] This uniform uniaxial flow-alignment of NLC director is commonly made by introducing NLC materials into liquid crystal slabs in the N phase. In our case, as shown in Figure 2a, starting from an initial state with low-density of randomly oriented TDs, the TDs never survive and a uniform unidirectional alignment of the director parallel to the dragging direction is realized. These results mean that the pattern formation needs sufficient number of TDs interacting collectively during the action of the flow. The detailed pattern forming conditions will be discussed later.

2000139 (2 of 9)
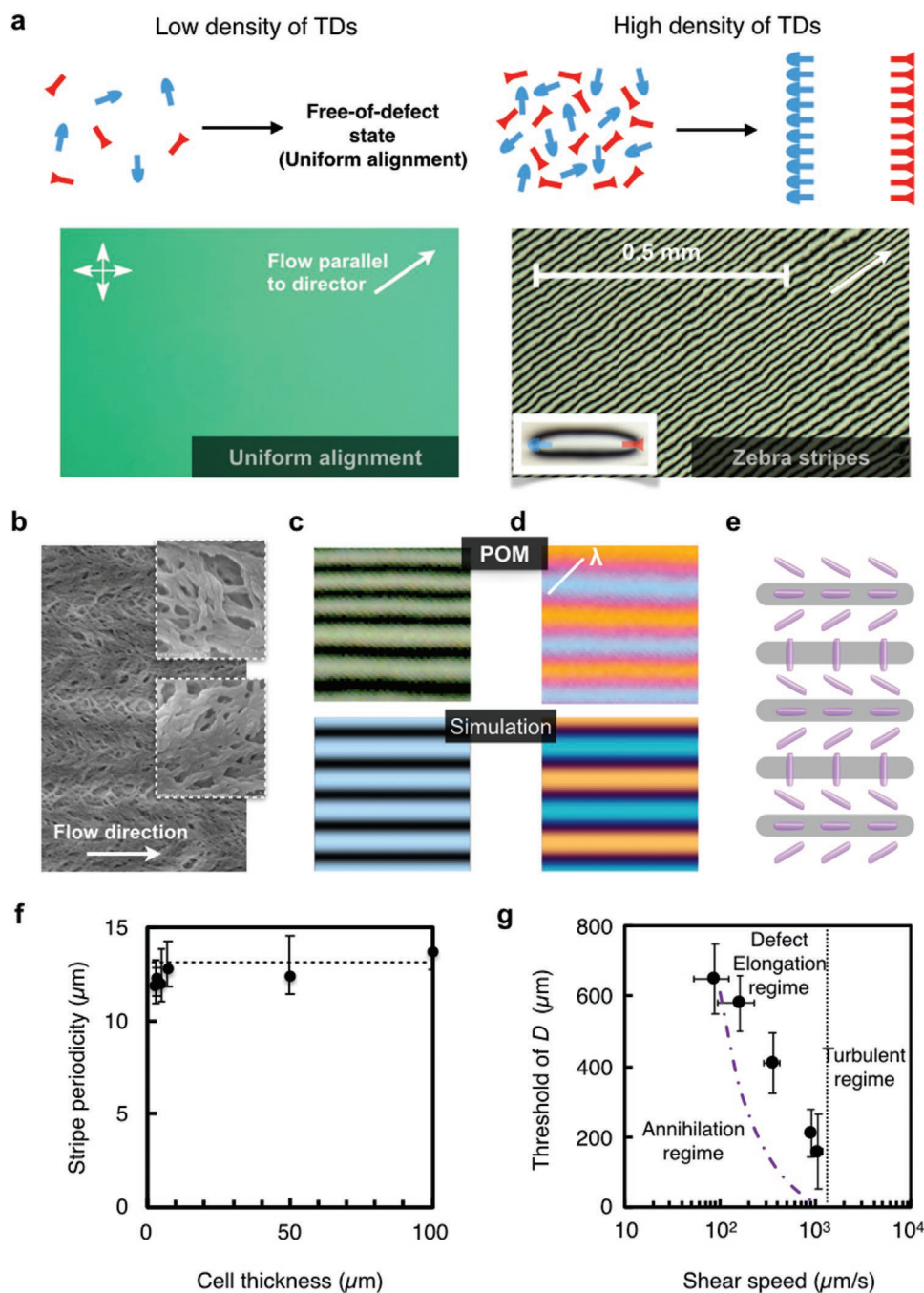
Figure 2. Conditions for fabricating topological patterns. a) Topological patterns formed at different initial densities of topological defects, along with schematics. The white arrows indicate the flow direction. Inset, the two ends of an elongated stripe are of one-half topological strength with opposite topological charge, i.e., one +1/2 and one −1/2. b) A polymerized film of the Zebra stripes formed at high density of topological defects. c) A detailed POM view and a simulated image of the Zebra stripes with crossed polarizers, and d) with a tint plate inserted. The simulation is made by the Jones Matrix method (Experimental Section). e) A schematic of the director field of the stripes. f) The cell thickness dependence of stripe periodicity. g) The minimal separation distance between two topological defects with opposite topological charges as a function of a shear speed measured by a rheometer with a calculated curve (purple dash-dotted line).

In order to directly visualize the spatial distribution of orientation of the topological pattern and to demonstrate the method for engineering topological polymer films by the current strategy, we fabricated a polymerized sample (Experimental Section) and observed its structure by scanning electron microscopy (SEM). A SEM image in Figure 2b visualizes that, distinct to a uniform state by simple flow-aligning, the director orientation keeps its average orientation parallel to the dragging direction but periodically oscillates in a splay mode. Such a deformation structure can be found in the so-called buckling

**ADVANCED
SCIENCE NEWS**

www.advancedsciencenews.com

**ADVANCED
MATERIALS
INTERFACES**

www.advmatinterfaces.de

instability in lamellar systems.[35] The maximum oscillation angle is about 40°. The periodicity of the orientational deformation is about 12 μm independent of the thickness of NLC films (Figure 2f), suggesting that no depth-dependent deformation of a twist of the director is present. This is also verified by independent observations: SEM images confirm that the maximum oscillation angle does not change at different depth positions; POM images confirm that the brushes of stripes (i.e., two dark brushes from one |1/2| disclination) are completely extincted, excluding the possibility of a severe twist deformation in the depth direction. These results can be understood as follows. When the stripes are created during the dragging process, a swarm of equally charged TDs arrange themselves to locate in a side-by-side manner (perpendicular to propagation direction, see Movie S2, Supporting Information). The topological swarming at the propagation front (i.e., Iso-N phase transition boundary) results in a mutual-repulsion between TDs. At a specific time, in the regime where the propagation front passed, the periodic stripes form and the azimuthal degeneracy of the planar surface is broken, resulting in a local easy axis being parallel to the director field revealed by SEM. Interestingly, though the produced anchoring after the dragging serves as a traditional surface that generates an elastic torque recovering the original striped state when the bulk director deviates by applying an external field, it is not a permeant but a memory state as will be discussed later. Figure 2c,d shows the corresponding POM images under crossed polarizers without and with a tint plate (i.e., λ-plate). Consistently with the director field observed by SEM, two features are confirmed: First, there are periodic dark lines where the director orientation is parallel to one polarizer running parallel to the dragging direction (Figure 2c); Second, the interference color of adjacent domains varies between orange and purple with a tint plate inserted (Figure 2d), which means the director orientation flips about the dragging direction. From these observations, we conclude that a zigzag director orientation field is achieved as shown in Figure 2e. In order to validate the assumed director field, we simulated the optical texture of the stripe pattern based on Jones matrices (Experimental Section), and obtained similar results compared to the experiments (Figure 2c,d).

Now, the key question is how the dragging speed affects the stability of the topological patterns. In order to test this, we statistically measure how the inter-distance, D, of a pair of TDs varies with dragging (shearing) speed created by using a rheometer (Anton Paar, MCR 502). We prepared a transparent quartz base plate with the AL1254 planar alignment layer coated, which allows us to observe textures from the beneath during the shearing (see the setup reported in ref. [36]). We find three regimes (Figure 2g): 1) Annihilation regime; 2) Defect elongation regime; 3) Turbulent regime. The Annihilation regime exists at low dragging speeds. In this regime, if the initial value of D is small, TDs generated at the phase transition attract mutually and finally disappear, irrespective of the initial density of TDs. The turbulent regime is located at high dragging speeds, where the dragging force is so strong that ordered distribution of TDs cannot be created. The Defect elongation regime that spontaneously stabilizes a pair of TDs with a topological charge of $|s| = 1/2$, rather than charges of integer-strength, lies between the Annihilation and the Turbulent

regimes. This is also confirmed by a direct flow injecting measurement (Section S1, Supporting Information). In this regime, both D and the dragging speed are large enough to disengage the cores of TDs. Therefore, TDs never annihilate and exist stably to form a straight elongated defect pair. They are the fundamental building blocks of the zigzag director orientational field observed in Figure 2a–e. It is worth noting that this can be described theoretically by accounting for the interaction between two TDs based on Dafermos's consideration[37] and assuming a viscous dragging force.[38] The viscous dragging force is described as $f_{drag} = 2\pi\eta v \ln(3.6/Er)$, where η, v, and Er are the kinematic viscosity, the velocity of the dragging and the Ericksen number, respectively.[39] By balancing f_{inter} and f_{drag}, the calculated ideal speed dependence of the distance above which a pair of TDs does not annihilate (a purple dash-dotted line) agrees, to some extent, with experimental data as overlaid in Figure 2g.

In order to design a characteristic dragging field for creating the corresponding nontrivial topological patterns, we adopt an electrotriggered spatial temperature gradient at low voltages as a source of the dragging field. **Figure 3**a shows the geometry of an NLC slab with one glass surface patterned with gold electrodes (gold triangles) on ITO-coated glasses (ITO heater). When the ITO electrodes are shorted and a DC or AC voltage is applied, a heating current is generated. Since the Au electrode has a much lower electric resistance than that of the ITO ones, the heating current flows mainly in the area between the two tips of the Au electrodes, leading to an ellipsoidal-shaped spatial distribution of temperature (Figure 3a,b).

We reduce the temperature of the heat sink at a rate of 1 K min⁻¹ (same result obtained in the range 0.1–10 K min⁻¹) while applying the voltage for local heating. This leads to a directional motion of the isotropic-nematic phase transition boundary with a velocity determined by the temperature gradient, $\Delta T/\Delta x$ (refer to the coordinates shown in Figure 3a). As a result, the isotropic-nematic boundary works for trapping the generated TDs and a dragging field (parallel to the direction of temperature gradient) for realizing the elongation of TD assemblies toward particular direction. It is expected that a larger temperature gradient prevents TDs from being generated randomly in space and facilitates the formation of topological patterns with higher ordering. Figure 3c–e shows an example of topological pattern generated at 2 V$_{pp}$ AC voltage that is created under a radial dragging field, an array of π-walls parallel to the temperature gradient field. Surprisingly, the defect cores at the end of each of π-walls are gathered in the middle of the slab but do not vanish (detailed dynamic generation processes are found in Movies S1 and S2, Supporting Information). They are all disclination lines aligning parallel to the surface normal with identical topological half-strength charge of +1/2, all the other −1/2 disclination lines are expelled from the middle. Such a self-sorting phenomenon of topological charges is observed for the first time and provides us valuable information about the forming process of the topological pattern. That is, upon the dragging of the isotropic-nematic phase transition boundary, +1/2 disclination lines move following the isotropic-nematic phase transition boundary faster than −1/2 disclination lines, leading to the self-sorting of the disclination lines. This fact is not contrary to the observation that two interacting oppositely
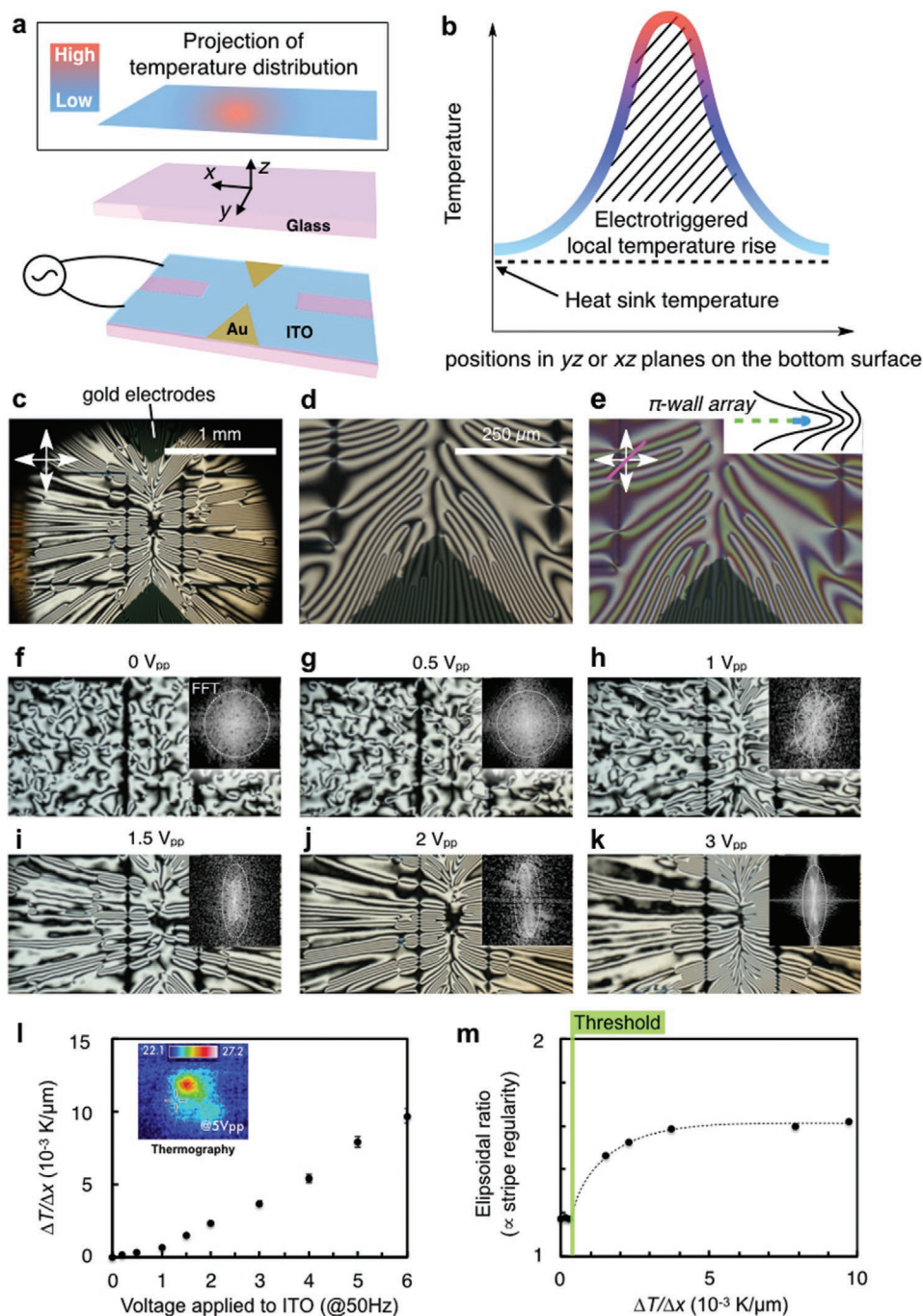
Figure 3. Design of topological network by patterned electrodes. a) A schematic of a liquid crystal slab with one surface patterned Au electrodes (gold colored) on ITO-coated (blue colored) glasses. The Au electrodes are shorted upon an application of an electric field. The temperature distribution in the space along either yz or xz planes are shown, where high and low temperature regimes are indicated by red and blue colors. b) A schematic of the temperature gradient along the A–A' plane in (a) is shown. c) A POM image of a topological pattern formed by using the liquid crystal slab as in (a) created at an AC field of $2V_{pp}$. d) An expanded view of (c). e) A POM view of (d) by inserting a tint-plate. f–k) Topological patterns generated at different AC voltage, along with their FFT images. l) Temperature gradient as a function of applied AC voltage. m) Ordering of topological patterns evaluated by the ellipsoidal ratio of the FFT of the patterns, which is proportional to the regularity, as a function of the temperature gradient. The ellipsoidal ratio is defined as the ratio of the full width at half maximum of the FFT images along the flow direction to the counterpart along the direction normal to the flow. The ellipsoidal ratio should be 1 for isotropic pattern and values larger than 1 for anisotropic patterns. The strength of the ordering is assumed to be proportional to the ellipsoidal ratio.

charged TDs move with different moving velocities caused by a backflow.[24,40] In that case, the backflow mainly originates from the reorientation of the local director field upon the

annihilation of the two TDs, and the flow depends on the sign of the spatial derivative of director field. In our case, at the early stage of self-sorting of the disclination lines, in addition to the

**ADVANCED
SCIENCE NEWS**
www.advancedsciencenews.com

**ADVANCED
MATERIALS
INTERFACES**
www.advmatinterfaces.de

above-mentioned flow, a directional biasing flow field should be also considered. The situation is very complicated, and the theoretical consideration will be reported elsewhere.

When the steepness of the temperature gradient is varied by changing the applied voltage, the pattern formation alters drastically. Figure 3f–k shows the generated patterns under POM at different voltages. Along with the corresponding FFT images, it is obvious that the regularity of the topological pattern becomes better by increasing the voltage. Further measurements and analyses of the correlations among applied voltage, temperature gradient (Figure 3l), dragging speed of TDs and regularity of the patterns reveal that, in order to create an ordered pattern, a certain threshold of temperature gradient, $\Delta T/\Delta x \approx 0.0003$ °C μm^{-1}, is needed (Figure 3m). Notably, ordered patterns cannot be achieved at low temperature gradient (i.e., $\Delta T/\Delta x < 0.0003$ °C μm^{-1}) because the speed of random nucleation is so high that TDs nucleate and orient randomly. On the other hand, above the threshold, the regularity continuously increases thanks to the suppression of the random nucleation of TDs, and saturates at about 0.004 °C μm^{-1}. Worth noting, the generated patterns are switchable to each other simply by heating the material to the Iso phase and rewriting the pattern at desired strength of an electric field.

As we stated earlier, unlike many other nonequilibrium topological pattern formations that relax after being free from external fields,[30–32] the nonvanishing nature is one of the key features for the present case. In order to test this further, we adopt a system, using a hydrophobic perfluoropolymer surface (Asahi Glass Corp., CYTOP), that enables to observe how the generated topological patterns change during both an isotropic-nematic phase transition and an anchoring transition (ATr) between planar and homeotropic surface alignments (director parallel and perpendicular to the substrates, respectively). Upon cooling the sample, the isotropic-nematic phase transition and the ATr (from planar to homeotropic) occur at 57 °C and 48 °C, respectively. The detailed transitional behavior can be found elsewhere.[41]

Figure 4 shows an annealing time-temperature diagram of topological patterns during the liquid-NLC phase transition. Raising up temperature from a state where surface anchoring of two slab substrates has a planar (P) orientation results in a complete melting of the initially generated topological pattern to the isotropic liquid (Iso) (Figure 4a-a"). Subsequent annealing the sample in the Iso state alters surface anchoring, thus leading to different types of patterns appearing when decreasing temperature again depending on the annealing time. Figure 4b-c" demonstrates two typical cases. When the annealing time is short enough (<30 s at 60 °C), the initial topological pattern (Figure 4a") is fully recovered (Figure 4b"). However, if the annealing time is longer than ≈10 min at 60 °C, random nucleation of TDs occurs. This leads to a final state with random director orientation when decreasing temperature from the Iso to the NLC state, evidenced by the Schlieren texture (Figure 4c"). These observations reveal that the surface anchoring, which tends to be randomized in its orientation during the annealing procedure in the Iso state, plays a key role in memorizing the generated topological pattern. Worth noting is that the topological pattern stably exists, if stored in the low-temperature NLC state.
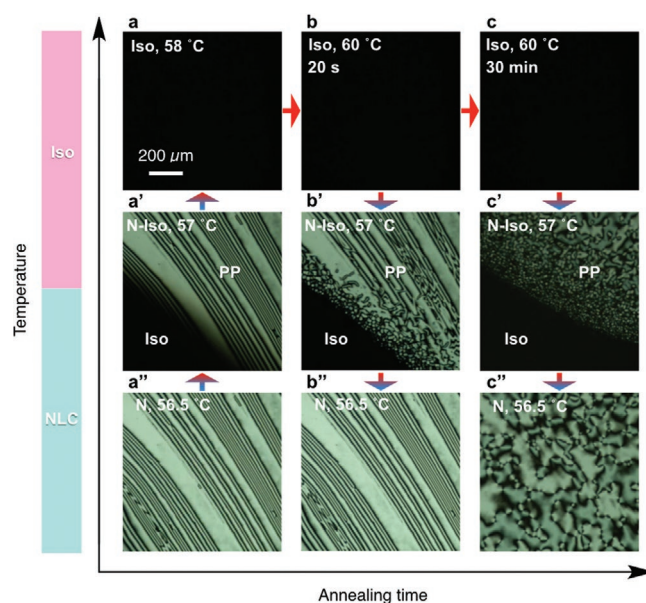
Figure 4. Orientational states of a liquid crystalline film with topological defect arrays upon cooling or heating, indicated by arrows, at different annealing time indicated in the corresponding images. The abbreviation of PP means the planar state realized on both surfaces.

While annealing samples in the Iso state acts as an eraser for the topological pattern, the reorientational behavior in a single NLC marginally affects the topological pattern, i.e., the topological pattern is memorized. **Figure 5** demonstrates the storage and regeneration processes of the topological pattern through the mentioned ATr, where the orientation angle of constituent molecules changes sharply by $\pi/2$ in a reversible manner.[41] Surprisingly, the random nucleation and growth of a new orientational state from an old orientational state does not affect the final regenerated topological pattern.

Lastly, in order to demonstrate the versatility of the flow-driven strategy for fabricating topological patterns, we applied the method to many other liquid crystalline phases such as chiral nematics or cholesterics (Ch), and smectics by introducing the materials into the liquid crystal slabs under the capillary force. **Figure 6**a shows a pattern that is made by flowing the material during the phase transition between the Iso and the Ch phase in a slab with homeotropic alignment. The stripes, called a fingerprint texture, run parallel to the flow direction, where the helical axis of the Ch material is perpendicular to the flow direction (cartoons of Figure 6a). This is a trivial pattern and a similar one can be obtained via the flow alignment effect by simply letting the Ch materials flow. The observed periodicity is determined by the helical pitch of the Ch phase. However, our method can also produce non-trivial patterns that cannot be made utilizing the conventional flow alignment effect. Figure 6b,c demonstrates two examples: SmA and SmC materials, where LC molecules form lamellar structures and their orientation are parallel and oblique to the layer normal of the lamellar structures, respectively. When only a flow is in act, a random swarm of focal conic defects appear and will be elongated along the flow direction for both SmA and SmC by the flow-alignment. However, the situation
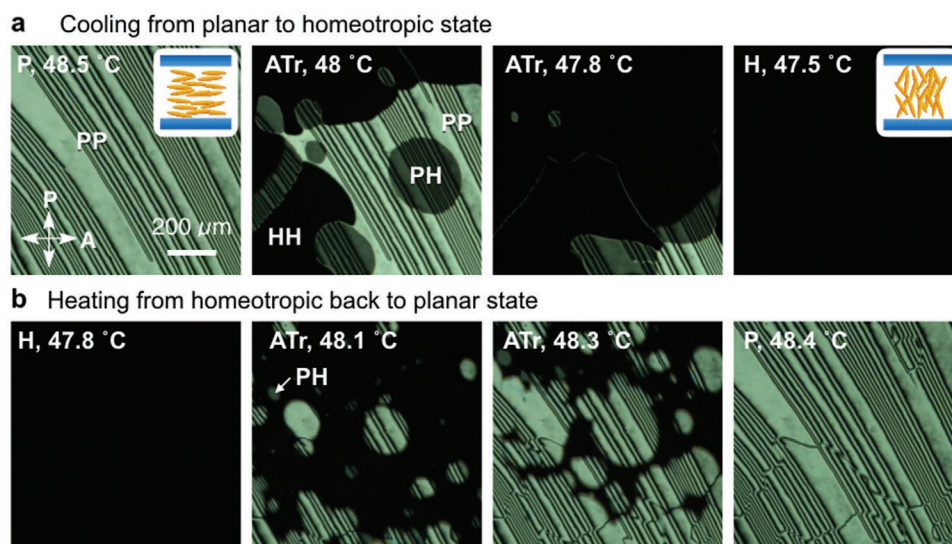
Figure 5. Orientational states of a liquid crystalline film with topological defect arrays upon a) cooling and b) heating between the homeotropic (H) and the planar (P) state in a single N phase. The abbreviations of different orientational combinations of PP, HH, and PH mean the planar state realized on both surfaces, the homeotropic state realized on both surfaces, and one surface in the planar state and the other in the homeotropic state. PP and HH states are exhibited with schematics.

changes when applying a flow during the phase transition of Iso-SmA or Iso-SmC. This realizes 2D periodic modulations of the molecular orientation, thus yielding new patterns as shown in Figure 6b,c. The periodic modulation in the SmC phase corresponds to a periodic precession of the c-director (i.e., the projection of the director onto the slab plane, cartoons of Figure 6b), which is an analogy to the 2D version of splay deformation of nematic director as presented above.
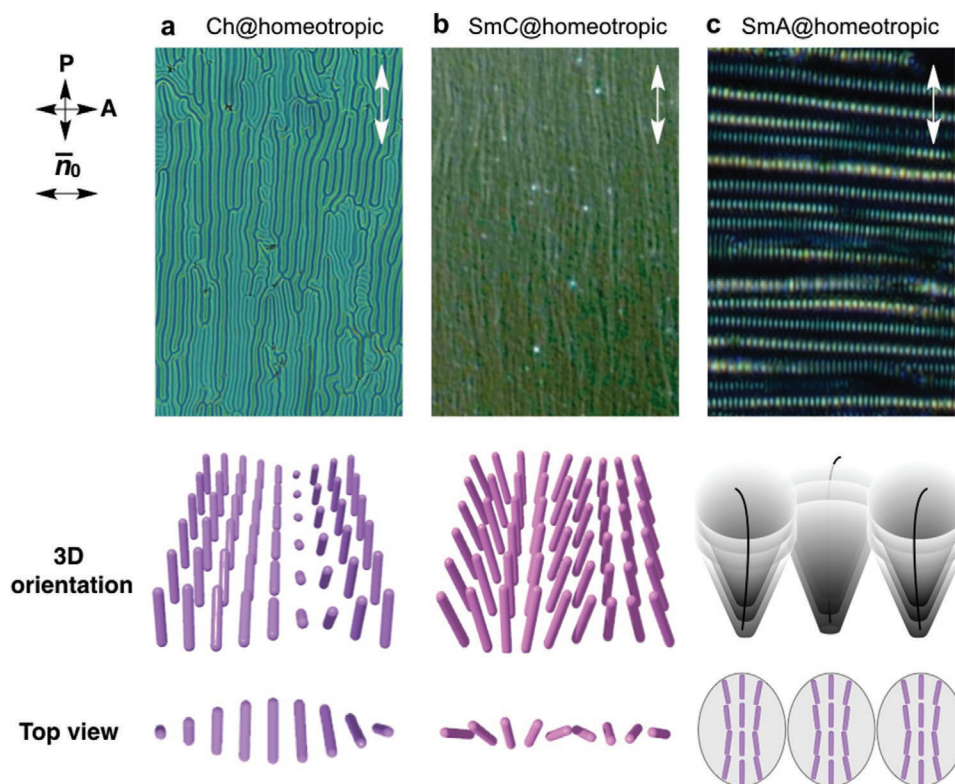
Figure 6. Topological patterns created through the coupling between a flow and the interactions between topological defects in different liquid crystalline phases: a) Ch phase, b) SmC phase, and c) SmA phase in the homeotropic boundary condition. The corresponding director field is shown. In the case of the SmA phase, the isosurface of the layers is depicted.

Stannarius and Harth reported similar pattern in a freely suspended SmC film by trapping point defects in a manmade hole.[42,43] The present strategy explains that such patterns can be controlled and generated in a large scale. Figure 6c presents the topological network made in the SmA phase. Remarkably, distorted focal conics are orderly aligned to a chain fashion perpendicular to the flow direction and equal inter-distance regimes (dark regimes with homeotropic alignment) exist between the focal conic chains. The arrays of the distorted focal conics are similar to what the SmA structure looks like under an electric field.[44] As shown in the cartoons of Figure 6c, the homeotropic regimes are transient regimes between two adjacent chains and are energetically favored.

In summary, we developed and demonstrated a strategy for processing topological defects and shaping topological patterns via a coupling between flow and the interactions between topological defects. The results suggest that the method can be applied to various types of materials. This work provides a facile methodology for designing more complex topological networks at a large scale. Further work is required to test the versatility of the strategy by combining microfluidic systems that can generate a variety of controllable flow fields.

Experimental Section

Materials: The main materials used to study the pattern formation are 4′-butyl-4-heptyl-bicyclohexyl-4-carbonitrile (CCN47, phase sequence upon cooling: Iso-57 °C-N-32 °C-SmA-25 °C-Crystal) for the N phase, a mixture of cyanobiphenyl and cyanoterphenyl components (E7, phase sequence upon cooling: Iso-58 °C-N) and a chiral dopant of (S)-2-Methylbutyl-4′-cyanobiphenyl (CB15) for the Ch phase, 4-n-decyl-biphenyl-4′-carbonitrile (10CB, phase sequence upon cooling: Iso-52 °C-SmA-43 °C-Crystal) for the SmA phase and 4-n-octyloxy-phenyl-4-n'-octyloxybenzoate (8OBE, phase sequence upon cooling: Iso-89 °C-N-72 °C-SmC-61 °C-Crystal) for the SmC phase. The materials exhibit direct Iso-N, Iso-Ch, Iso-SmA, and N-SmC phase transitions, respectively. The materials are sandwiched between a pair of glass substrates with proper surface treatment as explained for each specific case.

Preparation of Polymerized Film: The visualization of the orientation of local director is made by mixing a small amount of a photoreactive liquid crystalline monomer (1,4-Bis-[4-(3-acryloyloxypropyloxy)benzoyloxy]-2-methylbenzene (RM257, 9.7 wt%, Merck). A photoinitiator of IR651 (0.01%, Ciba) is added to the mixture to produce radical species to trigger the photopolymerization reaction. Once the pattern formation is completed, the fixation of the orientation of RM257 molecules is made by a photopolymerization procedure under a 365 nm UV irradiation.

Optical Calculation by Jones Matrix Method: POM images were simulated by the Jones matrix method.[45] Adapted to the actual conditions, the harmonic modulation of the azimuthal angle of the molecular alignment field was assumed as $\phi = \phi_0 \sin\left(\frac{2\pi}{\lambda}y\right)$, where $\varphi_0 = 40°$ and the wavelength of the stripes is $\lambda = 12$ μm. The y direction is perpendicular to the flow direction. The modulation of the director is assumed to be parallel to the y direction. The known value of the optical anisotropy of CCN47 was used, $\Delta n = n_e - n_0 \approx 0.03$.

Supporting Information

Supporting Information is available from the Wiley Online Library or from the author.

Conflict of Interest

The authors declare no conflict of interest.

[1] M. Chaikin, T. C. Lubensky, *Principles of Condensed Matter Physics*, Cambridge University Press, England **2000**.
[2] J. M. Kosterlitz, *Rev. Mod. Phys.* **2017**, *89*, 040501.
[3] H.-B. Braun, *Adv. Phys.* **2012**, *61*, 1.
[4] X. Wang, D. S. Miller, E. Bukusoglu, J. J. de Pablo, N. L. Abbott, *Nat. Mater.* **2016**, *15*, 106.
[5] Y. Sasaki, M. Ueda, K. V. Le, R. Amano, S. Sakane, S. Fujii, F. Araoka, H. Orihara, *Adv. Mater.* **2017**, *29*, 1703054.
[6] R. Barboza, U. Bortolozzo, G. Assanto, E. Vidal-Henriquez, M. G. Clerc, S. Residori, *Phys. Rev. Lett.* **2012**, *109*, 143901.
[7] Y. Ming, P. Chen, W. Ji, B. Wei, C. Lee, T. Lin, W. Hu, Y. Lu, *npj Quantum Mater.* **2017**, *2*, 6.
[8] R. Barboza, U. Bortolozzo, M. G. Clerc, S. Residori, E. Vidal-Henriquez, *Adv. Opt. Photonics* **2015**, *7*, 635.
[9] J. Kobashi, H. Yoshida, M. Ozaki, *Nat. Photonics* **2016**, *10*, 389.
[10] X. Yu, W. Koshibae, Y. Tokunaga, K. Shibata, Y. Taguchi, N. Nagaosa, Y. Tokura, *Nature* **2018**, *564*, 95.
[11] M. Zapotocky, L. Ramos, P. Poulin, T. C. Lubensky, D. A. Weitz, *Science* **1999**, *283*, 209.
[12] J. C. Loudet, P. Barois, P. Poulin, *Nature* **2000**, *407*, 611.
[13] U. Tkalec, M. Ravnik, S. Čopar, S. Žumer, I. Muševič, *Science* **2011**, *333*, 62.
[14] A. Nych, U. Ognysta, M. Škarabot, M. Ravnik, S. Žumer, I. Muševič, *Nat. Commun.* **2013**, *4*, 1489.
[15] H. Mundoor, B. Senyuk, I. I. Smalyukh, *Science* **2016**, *352*, 69.
[16] M. Wang, Y. Li, H. Yokoyama, *Nat. Commun.* **2017**, *8*, 388.
[17] H. Yoshida, K. Asakura, J. Fukuda, M. Ozaki, *Nat. Commun.* **2015**, *6*, 7180.
[18] L. Giomi, Z. Kos, M. Ravnik, A. Sengupta, *Proc. Natl. Acad. Sci. USA* **2017**, *114*, 5771.
[19] L. Lam, J. Prost, *Solitons in Liquid Crystals*, Springer Verlag, New York **1991**.
[20] I. Chuang, R. Durrer, N. Turok, B. Yurke, *Science* **1991**, *251*, 1336.
[21] M. J. Bowick, L. Chandar, E. A. Schiff, A. M. Srivastava, *Science* **1994**, *263*, 943.
[22] A. Pargellis, N. Turok, B. Yurke, *Phys. Rev. Lett.* **1991**, *67*, 1570.
[23] A. N. Pargellis, P. Finn, J. W. Goodby, P. Panizza, B. Yurke, P. E. Cladis, *Phys. Rev. A* **1992**, *46*, 7765.

[24] P. Oswald, J. Ignes-Mullol, *Phys. Rev. Lett.* **2005**, *95*, 027801.

[25] C. Blanc, D. Svensek, S. Zumer, M. Nobili, *Phys. Rev. Lett.* **2005**, *95*, 097802.

[26] R. Stannarius, C. Bohley, A. Eremin, *Phys. Rev. Lett.* **2006**, *97*, 097802.

[27] I. Dierking, M. Ravnik, E. Lark, J. Healey, G. P. Alexander, J. M. Yeomans, *Phys. Rev. E* **2012**, *85*, 021703.

[28] R. R. Guimaraes, R. S. Mendes, P. R. G. Fernandes, H. Mukai, *J. Phys.: Condens. Matter* **2013**, *25*, 404203.

[29] Y.-K. Kim, S. V. Shiyanovskiiand, O. D. Lavrentovich, *J. Phys.: Condens. Matter* **2013**, *25*, 404202.

[30] A. Buka, L. Kramer, *Pattern Formation in Liquid Crystals*, Springer, New York **1996**.

[31] P. Pieranski, M. H. Godinho, *Soft Matter* **2019**, *15*, 1469.

[32] P. Pieranski, J. P. Hulin, M. H. Godinho, *Eur. Phys. J. E* **2017**, *40*, 109.

[33] A. Doostmohammadi, M. F. Adamer, S. P. Thampi, J. M. Yeomans, *Nat. Commun.* **2016**, *7*, 10557.

[34] K. Skarp, S. T. Lagerwall, B. Stebler, D. McQueen, *Phys. Scr.* **1979**, *19*, 339.

[35] J. P. Courbin, J. Delville, J. Rouch, P. Panizza, *Phys. Rev. Lett.* **2002**, *89*, 148305.

[36] S. Aya, A. Jákli, C. T. Imrie, Á. Buka, F. Araoka, in *Proc. SPIE, Liquid Crystals XXII*, SPIE, Bellingham, WA **2018**, p. 107350Z.

[37] C. M. Dafermos, Q. J. Mech, *Appl. Math.* **1970**, *23*, 49.

[38] M. Kleman, O. D. Lavrentovich, *Soft Matter Physics: An Introduction*, Springer Verlag, New York **2003**.

[39] R. Larson, D. Mead, *Liq. Cryst.* **1993**, *15*, 151.

[40] G. Tóth, C. Denniston, J. M. Yeomans, *Phys. Rev. Lett.* **2002**, *88*, 105504.

[41] S. Aya, Y. Sasaki, H. Takezoe, K. Ishikawa, K. Ema, T. Hikima, M. Takata, F. Araoka, *Langmuir* **2016**, *32*, 10545.

[42] K. Harth, R. Stannarius, *Eur. Phys. J. E* **2009**, *28*, 265.

[43] R. Stannarius, K. Harth, *Phys. Rev. Lett.* **2016**, *117*, 157801.

[44] A. Suh, H. Ahn, T. J. Shin, D. K. Yoon, *J. Mater. Chem. C* **2019**, *7*, 1713.

[45] R. C. Jones, *J. Opt. Soc. Am.* **1941**, *31*, 488.